

# Vertical Takeoff and Landing of Flexible Wing Kite Power Systems

Sebastian Rapp\* and Roland Schmehl†  
*Delft University of Technology, Faculty of Aerospace Engineering*

**In this work vertical take-off and landing capabilities of flexible wing kite power systems are investigated. Employing a mast-based launching and landing concept the operational envelope will be enlarged using a novel multicopter based launching approach. The multicopter guides the kite along a specified launching path until the operational altitude is reached. Mast based and drone assisted launching and landing maneuvers are compared in a developed simulation environment. Different scenarios in turbulent wind fields are used to analyze the general feasibility of the proposed concept and its benefits compared to existing approaches.**

## I. Introduction

ONE of the technical challenges of airborne wind energy (AWE) is the automated launching and landing of the airborne subsystem [1]. To ensure the commercial viability of the technology, these processes, which envelope the operational phase of the system, have to be highly reliable and robust at all possibly occurring weather conditions. However, as an atmospheric phenomenon, wind is fluctuating in magnitude and direction, on short and long time scales, which makes launching and landing in particular challenging. For most of the practically pursued system concepts the launching starts from a configuration at which the tether is short and the airborne device is consequently close to the ground station. Because of the wind shear effect the wind velocities at ground level are generally low and the turbulence level is high, both conditions negatively affecting the robustness of the launching and landing phases. The low dynamic pressure in ground proximity, due to low wind speeds and low kinematic speed of the kite itself, leads to a limited steering authority. This makes the control system design in particular challenging.

Automatic vertical take-off and landing (VTOL) is a promising approach and has been demonstrated successfully by several companies in the AWE field that operate rigid wing kite power systems e.g. [2–5]. VTOL has several advantages over horizontal or rotational takeoff and landing concepts both from a system engineering but also from a control point of view.

First, the required additional infrastructure for a VTOL system is negligibly small and comparably simple since no additional mast, rotating platform or rotating arm is required. This makes the VTOL approach a cheaper and more mobile solution compared to other concepts.

Second, the system can be launched in an arbitrary direction, which is not possible if a horizontal take-off approach is chosen unless the corresponding launching platform can be rotated, which of course increases the complexity and cost.

Third, precise landing maneuvers are possible in a reliable manner. The wing can be pulled towards the ground station while the rotor thrusts can be used to stabilize the tethered hover equilibrium. It is hence straightforward to control a precise landing

---

\*PhD Researcher, Delft University of Technology, Kluyverweg 1, 2629HS, Delft, The Netherlands, s.rapp@tudelft.nl.

†Associate Professor, Delft University of Technology, Kluyverweg 1, 2629HS, Delft, The Netherlands, r.schmehl@tudelft.nl.

maneuver without requiring additional sensor equipment (e.g. cameras).

A more detailed comparison of different landing approaches for rigid wing kite power systems can be found in [6].

Companies with flexible wing systems have tested several different launching and landing strategies including simple static mast based launch and landing [7], upside down swing-up launching [8] or launching systems based on a rotating arm [9]. All these systems depend heavily on the wind conditions in ground proximity, hence have a limited operational envelope, do not scale well and their reliability is difficult to prove.

In general, a pure VTOL approach for flexible kites leads to additional technical challenges since the rotors are difficult to integrate into the wing. In [10] the rotors are instead mounted on the steering unit and the kite is dragged upside down to the operational altitude. The downside of this approach is the required on-board power which is necessary to compensate kite weight as well as the aerodynamic forces. Moreover the additional mass has to be carried on board during power production, which has a negative impact on the overall system performance. Furthermore, scalability issues arise for larger kites that generate large aerodynamic forces that might be difficult to compensate by the on-board power of the multicopter system. The approach proposed in this work will suffer less from the scalability problem, since the higher aerodynamic forces generated by larger kites can be explicitly exploited during the launching.

Besides the work in [10] the potential of vertical launching and landing of flexible kite power system has not been addressed in the scientific community in detail yet. This work tries to fill this gap by proposing a hybrid VTOL approach. It consists of a static mast based approach, whose operational envelope will be extended by utilizing an externally attached multicopter system to pull the kite to the operational altitude in certain wind conditions that would not allow a passive mast based launch. In case of sufficiently high ground wind speed the kite will be launched without the external assistance of the multicopter.

This work builds on the static feasibility analysis as presented in [10] to size the required VTOL system such that it is able to launch one of the currently operated flexible kite power systems of TU Delft. In contrast to the approach in [10] the VTOL system is not integrated into the kite system but instead will be separated after the kite is launched. Photographic footage of the first experimental explorations of this concept is shown in figure 1.



**Fig. 1 Custom made drone launching a 9 m<sup>2</sup> kite. Photo credits: Marcos Jerez Venegas.**

A fully automated launching with separate VTOL and kite system is challenging due to the required automation of the attachment process. In this work the requirement for full autonomy will be weakened, such that a manual attachment of the drone still

complies with the system requirements. The overall goal will be to increase the operational envelope using external thrust assistance during the launching phase, while the landing is carried out without external assistance besides the pulling force controlled by the winch. This setup would allow a combination of a mast based launching system as performed by [7] with the VTOL setup. Both concepts can be regarded as complimentary since the static mast based launching is appealing due to its simplicity and autonomy with the disadvantage that it works only with a sufficiently high ground wind speed, whereas the VTOL concept works most reliably in low wind condition in ground proximity at the cost of increased complexity.

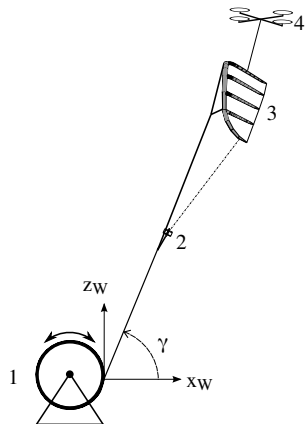


**Fig. 2 Schematic figure of the drone assisted launching approach with ground station 1, kite steering unit 2, kite 3 and drone 4. The origin of the wind frame  $W$  is defined at the tether release point at the winch. The launching path angle is denoted as  $\gamma$ .**

The paper is structured as follows. In section II a detailed theoretical analysis is conducted with the aim to develop boundary conditions for the launching and landing phase. In section III simulation models for all the involved subsystems are developed. For each of the subsystems a controller is designed in section IV. Simulation results will be presented in section V. The paper concludes with an overview of the developed methodology and proposes further research directions in section VI.

## II. Theoretical Analysis

### A. Boundaries of Assisted and Non-assisted Launching and Landing Maneuvers

For the subsequent analysis the kite will be regarded as a pointmass. Furthermore, the following calculations require the definitions of additional coordinate systems. The wind frame  $W$  will be used to define the position of the kite and is defined as shown in figure 2, where the  $x_w$  is pointing in downwind direction and the  $z_w$  axis is pointing upwards. The tangential plane frame  $T$  will be used in combination with a bodyfixed frame to describe the orientation of the kite. Figure 3 shows the definitions of the  $T$  as well as the  $B$  frame, which are both attached to the center of gravity of the kite. The  $z_T$  axis is pointing towards the origin of the wind frame  $W$ , the  $y_T$  is parallel to the  $y_w$  frame (both not displayed in the figure), and the  $x_T$  axis forms an orthonormal basis with  $x_T$  and  $z_T$ . The body fixed axis  $x_B$  axis is aligned with the center chord of the wing, while the  $z_B$  axis points from the origin of the  $B$  frame towards the steering unit. Note, that in the following analysis the steering unit is assumed to coincide with the center of gravity. Strictly speaking, the orientation of a point mass is not defined, however it will be shown that the definition of a pitch angle  $\Theta_T$  is paramount to obtain less conservative results in the subsequent analysis, hence the pitch angle can be regarded as an angle

about which the wing is rotated relatively to the tangential plane frame. In reality this rotation is mainly caused by the drag and weight of tether and steering unit.

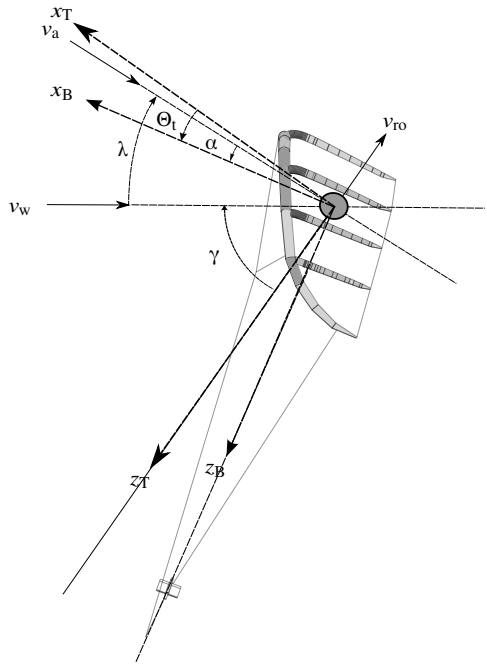


**Fig. 3** The figure contains a side view of the tangential plane frame  $T$  and body fixed frame  $B$  as well as the definitions for pitch angle  $\Theta_T$ , angle of attack  $\alpha$ , path angle  $\gamma$  as well as the angle between the apparent wind speed vector  $v_a$  and the wind speed vector  $v_w$ ,  $\lambda$ . Note that for better readability the velocity vectors are not displayed in the right scale.

A kite that is not flying crosswind can have an equilibrium position for sufficiently high wind speeds in downwind direction at a certain elevation angle. This equilibrium is often denoted parking position in the airborne wind energy literature [1]. Most publications regarding flight control of kites assume that the kite is already airborne and the existing control approaches usually start controlling the kite from the parking position into crosswind flight and back. The work in this paper aims to fill this gap by providing a methodology that guides the kite from the ground to the parking position and from the parking position back to the ground. Due to the modularity, the presented approach can later on be combined with existing crosswind flight controllers effortlessly.

The goal of the kite launching maneuver will be to control the kite from the ground to the parking position either assisted by the drone or non-assisted depending on the wind conditions. Since the wind speed can be related to altitude a relationship between the wind speed and the parking elevation angle can be derived. The parking equilibrium state can be calculated using a moment equilibrium around the tether exit point on the ground. The contributing forces are the aerodynamic force  $(\mathbf{F}_a)_A$  consisting of drag  $D$  and lift force  $L$  and the weight of the kite  $(\mathbf{F}_g)_W$ . The tether force is not appearing in the equilibrium since it is assumed that the tether is straight in this analysis. In the parking position the kinematic velocity of the kite is zero, hence  $v_a = v_w$ , where  $v_w$  is the wind speed at the parking altitude. The equilibrium elevation angle is then given by

$$\tan(\beta) - \frac{L(\beta) - m \cdot g}{D(\beta)} \stackrel{!}{=} 0 \tag{1}$$

with

$$L = 0.5 \cdot \rho \cdot S_k \cdot C_L(\alpha) \cdot v_w^2 \quad (2)$$

$$D = 0.5 \cdot \rho \cdot S_k \cdot C_D(\alpha) \cdot v_w^2 \quad (3)$$

and

$$\beta = \frac{\pi}{2} - \alpha + \theta_t, \quad (4)$$

where  $\Theta_t$  is the pitch angle of the kite with respect to the tangential plane and  $\rho$  is the air density and  $S_k$  is the kite reference area. For  $C_L(\alpha)$  and  $C_D(\alpha)$  the same values as in [11] are used. Equation (1) depends implicitly on  $\beta$ , hence it has to be solved numerically. In figure 4 the solutions of equation (1) for different wind speeds and pitch angles are visualized in a contour plot, where the contour lines represent the parking elevation angles. Note that due to operational constraints a minimum elevation angle

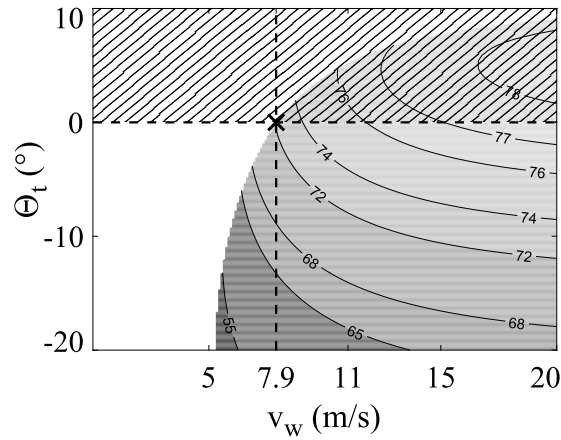


**Fig. 4** Theoretical equilibrium parking elevation angle in dependency of the kite pitch angle  $\Theta_t$  and the wind speed  $v_w$ . The contour lines indicate the parking elevation angle. The result is obtained using a moment equilibrium around the ground station for different wind speeds and kite pitch angles. In practice, positive pitch angles during parking are not achieved, which is indicated by the hatched rectangular area. The cross indicates the minimum wind speed  $v_w \approx 7.9 \frac{m}{s}$  with  $\Theta_t = 0^\circ$  and  $\beta \approx 72^\circ$ .

of approximately  $45^\circ$  is imposed. Since in practice positive pitch angles are not obtained the mathematical solutions in the hatched area are practically not feasible. It can be observed that depending on the kite pitch angle  $\Theta_t$  different minimal wind speeds result, which usually range from  $-5.4 \frac{m}{s}$  with  $\Theta_t = -20^\circ$  to  $\approx -8 \frac{m}{s}$  with  $\Theta_t = 0^\circ$ . For the subsequent launching and landing analysis it is beneficial to look at equilibrium points with a constant radial velocity, denoted as  $v_{ro}$  in the following. This enables to calculate boundaries that would allow a non-assisted launching maneuver. In this case the apparent wind speed depends also on the reeling out speed  $v_{ro}$  according to

$$\mathbf{v}_a = \mathbf{v}_w - \mathbf{v}_{ro} \quad (5)$$

This changes also the implicit expression for the moment equilibrium. Assuming again a straight tether the moment equilibrium for

an arbitrary reeling out velocity  $v_{ro}$  is given by

$$0 = \mathbf{r}_G(\beta) \times (\mathbf{F}_a(\beta) + \mathbf{F}_g) \quad (6)$$

with

$$\beta = \frac{\pi}{2} - \lambda - \alpha + \theta_t, \quad (7)$$

and

$$\lambda = \arccos\left(\frac{\mathbf{v}_a^\top \mathbf{v}_w}{\|\mathbf{v}_a\|_2 \|\mathbf{v}_w\|_2}\right) \quad (8)$$

All appearing vectors are given in the wind frame  $W$ . Solving equation (6) numerically for different wind speeds and reeling out velocities yields the static equilibrium elevation angles depicted in the contour plot of figure 5. Note the consistency to the parking

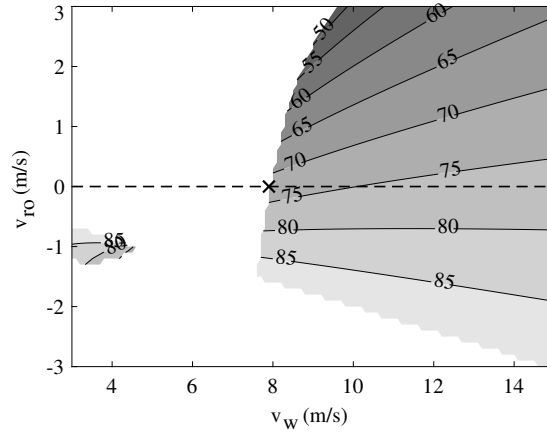


**Fig. 5** Equilibrium elevation angles for different reeling in and out velocities  $v_{ro}$  and wind speeds  $v_w$ . The result is obtained from a moment equilibrium similar to the results in figure 4 but with a constant reeling out or reeling in velocity. The pitch angle  $\Theta_t$  is assumed to be zero. Only solution with an angle of attack  $0 \leq \alpha \leq 30^\circ$  are displayed as feasible solutions. High reeling in velocities can lead to an overshoot i.e.  $\beta > 90^\circ$

equilibrium elevation angle at  $v_{ro} = 0$  with  $\Theta_t = 0$  indicated by the cross. The induced conservatism that comes along with the assumption  $\Theta_t = 0$  will be discussed in the following. Based on the results in 5 an additional requirement for the non-assisted kite launching becomes visible. It can be observed that a kite attached to a vertical mast i.e.  $\beta = 90^\circ$  is not within the depicted feasible solution space. If for instance the kite is launched with  $v_{ro} = 0.5 \frac{m}{s}$  a wind speed of  $v_w \leq 8.1 \frac{m}{s}$  and additionally an initial inclination  $\beta = 67^\circ$  is required otherwise no quasi-steady launching is possible. For arbitrary reeling out velocities  $v_{ro} > 0$  the wind speed and elevation angles have to satisfy  $v_w > 8 \frac{m}{s}$  and  $\beta < 72^\circ$ , respectively, in order to enable a non-assisted launching.

In theory, the reeling out velocity determines the required initial inclination of the kite for a given wind speed. The choice for the reeling out velocity for a given wind speed is a design parameter and could be determined based on the to be expected parking elevation angle. As can be observed in figure 5, for a given wind speed, decreasing the reeling out velocity will increase the equilibrium elevation angle. For instance, assuming that just before the target altitude a wind speed of  $v_w = 11 \frac{m}{s}$  is present and assuming that the kite is launched quasi-steady with  $v_{ro} = 1 \frac{m}{s}$ , then stopping reeling out i.e.  $v_{ro} \rightarrow 0$  creates a velocity component perpendicular to the radial velocity  $v_{ro}$ , since the equilibrium elevation angle increases up to approximately  $76^\circ$ . Looking at figure

4 it can be observed that for  $\Theta_t \in (-10^\circ, 0^\circ)$ , which is the usually range of the pitch angle observed during experiments and wind speeds  $v_w > 8 \frac{m}{s}$ , which is required for non-assisted kite launches, the parking elevation angle will be greater then  $72^\circ$ , while the maximum elevation angle will be around  $77^\circ$  for  $v_w = 15m/s$ .

Depending on the desired conservatism launching path elevation angles up to  $72^\circ$  are possible, since it is desired that the kite will move in positive  $x_T$  if the reeling out stops. Note that in the case of  $\Theta_t = 0$ , which is in practice not achievable the equilibrium path angle during the launching will always be smaller than the parking elevation angle, hence the maximum reeling out speed is theoretically determined by an operational constraint regarding the minimum elevation angle during launching. This however also requires higher wind speeds to compensate the loss in apparent wind speed with increasing reeling out speeds. The smallest reeling out speed is essentially limited by other operational constraints such as requirements on the launching time or the accuracy of the winch controller at low rotational speeds. It is assumed that in practice the reeling out speed will be in the interval between  $0.5m/s$  and  $1.0m/s$ , which requires a wind speed between  $8.1m/s$  and  $8.3m/s$  for a launch along equilibrium points.

The presented results so far are conservative due to the assumption of  $\Theta_t = 0$ . However in reality it has been observed that usually  $\Theta_t \in (-10^\circ, 0)$ . For instance, if a pitch angle of  $\Theta_t = -7.5^\circ$  is assumed the minimum wind speed is reduced to  $6.2 \frac{m}{s}$  in the limiting case of  $v_{ro} = 0$ .

The contour plot for the case with  $\Theta_t = -7.5^\circ$  is depicted in figure 6.

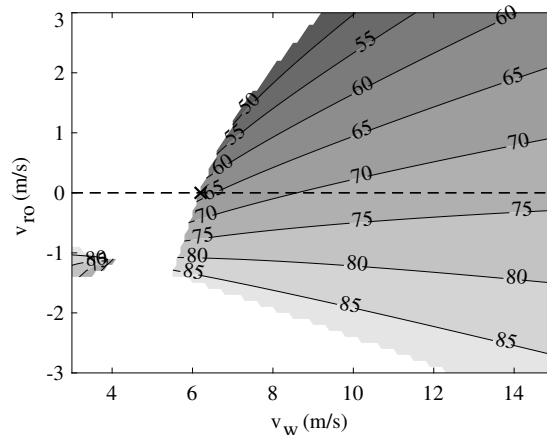


**Fig. 6** Equilibrium elevation angles for different reeling out and reeling in velocities  $v_{ro}$  and wind speeds  $v_w$ . The equilibrium points are obtained with  $\Theta_t = -7.5^\circ$ . Only solution with an angle of attack  $0 \leq \alpha \leq 30^\circ$  are displayed as feasible solutions. The minimum wind speed with a constant tether length is indicated by the cross. Comparing the results with figure 5 shows the conservatism of the assumption  $\Theta_t = 0$ .

This clearly shows that for a non-conservative estimation of equilibrium points the pitch angle of the kite plays a major role. Since the pitch of the kite is mainly influenced by the tether drag and steering unit weight, the simple point mass model is not sufficient to calculate real bounds, but due to the conservatism leads to safe bounds. Including the tether drag and weight of the steering unit in the equilibrium points is part of future research.

Similar consideration can be made regarding a quasi-steady landing. Quasi-steady solutions with  $v_{ro}$  are again depicted in figure 5. Note, that in the simulation only angles of attack up to  $30^\circ$  are simulated, hence only steady solutions that comply with this requirement are displayed. Comparing the results in figure 5 with the results in 6 shows that also in case of  $v_{ro}$  negative pitch angles lead to less conservative results. Depending on the wind measurement conservative reeling-in speeds can be selected.

Although it is likely that the wind speed as measured on the ground is lower than the wind speed at the kite itself, the kite will reach an equilibrium at higher elevation angles. Note that if a reeling-in speed higher than the recommended speed based on 5 is chosen, the resulting elevation angle could violate the constraint  $\beta < 90^\circ$  which results in an overshoot of the kite with respect to the ground station.

## B. Quadcopter performance definition

In this section the required power of the multicopter will be estimated based on the flight time as well as the mass of the kite and tether.

According to [10] the required power  $P_{t,e}$  to lift a certain mass with a multicopter system can be estimated based on momentum theory. It essentially depends on efficiency factor  $\eta_e$ , launching time  $t_L$ , battery energy density  $\gamma_E$ , mass for electronics and airframe frame  $m_0$ , kite mass  $m_k$ , tether mass  $m_t$ , power to mass ratio  $\lambda_M$ , gravity  $g$ , air density  $\rho$ , as well as the total swept rotor area  $A_p$ . Following the steps in [10] an implicit expression for  $P_{t,e}$  can be derived, which is given by

$$P_{t,e} = \frac{1}{\eta_e} \sqrt{\frac{\left(\left(\frac{P_{t,e}t_L}{\gamma_E} + m_0 + m_k + m_t + P_{t,e}\lambda_M\right)g\lambda\right)^3}{2\rho A_p}} \quad (9)$$

This expression can be solved numerically for  $P_{tot,e}$ . Eventually, the battery mass can be calculated according to

$$m_B = \frac{P_{t,e}t_L}{\gamma_E} \quad (10)$$

The chosen numerical values in this work are summarized in table 1 and 2. Kite specific parameters are obtained from [11].

**Table 1 Design parameters**

$\gamma_E$ , Wh/kg	$m_k$ , kg	$m_t$ , kg	$A_p$ , $m^2$	$\lambda_m$ , kg/kW
130	14.61	1.3	0.28	0.2

**Table 2 Design parameters**

$m_0$ , kg	$\rho$ , $kg/m^3$	$\lambda$ , -	$g$ , $m/s^2$	$\eta_e$ , -	$t_L$ , min
0.5	1.225	1.2	9.81	0.8	3

The values for  $\gamma_E$ ,  $A_p$ ,  $\lambda_m$ ,  $m_0$ , and  $\eta_{eff}$  are obtained from [10]. A mean launching velocity of  $1m/s$  and a mean launching time of  $3min$  has been chosen in this work. Note that an additional flight time has to be added during which the drone will land after the kite has been launched, which is estimated to be  $\approx 1min$ . It turns out that the additional required power for the drone landing can be neglected and will be captured by the conservative estimation for the required power during the kite launching phase. The thrust to weight ratio  $\lambda_m$  seems to be reasonable since no highly dynamic flight paths will be flown and in addition the kite will compensate partially its own weight with lift. For the kite specific parameters the values of the HYDRA kite of TU Delft are chosen. Note that all the design values will be used later in the nonlinear simulation to assess their feasibility.

Solving equation 9 with the values in table 1 and 2 yields a required power of  $P_{tot,e} = 6.6kW$  which leads to a battery mass of  $m_B = 2.5kg$  and motor mass of  $m_M = 1.3kg$  using the assumed power to weight ratio  $\lambda_M$ . This leads to an overall drone weight of  $m_{drone} = m_0 + m_B + m_M = 4.3kg$ .

### III. Simulation models

In this section the simulation models for kite, tether, drone and ground station will be presented.

#### A. Quadcopter

The drone is modeled as a rigid body with three degrees of freedom. The rotational dynamics have been neglected so far, since they do not have a major influence on the presented results in this paper. This is especially due to the fact that in this application no high dynamic maneuvers are flown and the drone remains most of the time in a quasi-hover state. This reduces also the required system parameters to the quadcopter mass only, if aerodynamic effects of the drone are neglected. A more refined model will be included in the simulation framework in the future. The governing equations of motion are given by Newton's second law of motion [? ]. This yields for the translational dynamics in the Wind frame  $W$

$$\begin{aligned} (\dot{\mathbf{p}}^G)_W &= (\mathbf{v}_{k,D}^G)_W \\ (\dot{\mathbf{v}}_{k,D}^G)_W &= \frac{1}{m_{drone}} \cdot (\mathbf{F}_{tot}^G)_W \end{aligned} \quad (11)$$

where  $(\mathbf{p}^G)_W \in \mathbb{R}^{3 \times 1}$  and  $(\mathbf{v}_{k,D}^G)_W \in \mathbb{R}^{3 \times 1}$  represent the position and kinematic velocity of the center of gravity in the Wind frame, respectively. The total force vector  $(\mathbf{F}_{tot}^G)_W$  can be split into

$$(\mathbf{F}_{tot}^G)_W = (\mathbf{F}_a^G)_W + (\mathbf{F}_g^G)_W + k \cdot (\mathbf{F}_t^G)_W + (\mathbf{F}_p^G)_W + (\mathbf{F}_d^G)_W, \quad (12)$$

where  $(\mathbf{F}_a^G)_W$  represents the aerodynamic force,  $(\mathbf{F}_g^G)_W$  represent the gravitational force,  $(\mathbf{F}_t^G)_W$  represents the force that is transmitted by the tether between kite and drone,  $(\mathbf{F}_p^G)_W$  represents the propulsion force, and  $(\mathbf{F}_d^G)_W$  represents an arbitrary disturbance. Note,  $k$  is zero if kite and drone are detached. Usually the aerodynamic force acting on the quadcopter is negligible especially in the slow speed regime the quadcopter is flying in this application. The gravitational force is given by

$$(\mathbf{F}_g^G)_W = \begin{pmatrix} 0 & 0 & -m_{drone} \cdot g \end{pmatrix}_W^T \quad (13)$$

The propulsion force represent the resulting thrust of the contributing four rotors. Assuming that the thrust vectors are acting perpendicularly to the  $x_B, y_B$  plane of the quadcopter body fixed frame  $B$ , the propulsion force vector in the wind frame is given by

$$(\mathbf{F}_p^G)_W = \mathbf{M}_{WB} \cdot \begin{pmatrix} 0 & 0 & T \end{pmatrix}_W^T, \quad (14)$$

where  $T$  is given by

$$T = \sum_{i=1}^n F_{t,i}. \quad (15)$$

The matrix  $\mathbf{M}_{WB} \in \mathbb{R}^{3 \times 3}$  transforms a vector from the  $B$  frame into the  $W$  frame. Note, in this work the actuator dynamics are not modeled hence the required moments are directly mapped to the required thrust forces. The connection between the kite and drone is modeled as a spring-damper element. Mathematically it will be defined as

$$\begin{aligned} \left(\mathbf{F}_t^G\right)_W &= \mu(e) (k (e - l_s) + \\ &\quad d \left(\mathbf{t}^{KD}\right)_W^T \left( \left(\mathbf{v}_{k,D}^G\right)_W - \left(\mathbf{v}_{k,K}^G\right)_W \right) \left(\mathbf{t}^{KD}\right)_W \end{aligned} \quad (16)$$

with the Euclidean distance between kite and drone

$$e = \left\| \left(\mathbf{p}_D^G\right)_W - \left(\mathbf{p}_K^G\right)_W \right\|_2, \quad (17)$$

the direction vector of the tether force

$$\left(\mathbf{t}^{KD}\right)_W = \frac{\left(\mathbf{p}_D^G\right)_W - \left(\mathbf{p}_K^G\right)_W}{\left\| \left(\mathbf{p}_D^G\right)_W - \left(\mathbf{p}_K^G\right)_W \right\|_2}, \quad (18)$$

and a smoothed heavyside function  $\mu(\epsilon)$  that drives the tether force to zero whenever the tether is not fully stretched. The smoothing turns out to be numerically more efficient, since the tether force does not change infinitely fast between the taut and loose tether state.

$$\mu(e) = \min \left( \max \left( \frac{1}{\Delta} e + 1, 0 \right), 1 \right) \quad (19)$$

## B. Kite

The dynamics of the kite are implemented in the simulation framework according to [11]. A short overview of the model will be given in the following. For a detailed derivation of the equations of motion please refer to [11]. The kite is modeled as a four point particle system, where the individual particles are connected by spring-damper elements. The shape of the kite is approxiamted by two sidesurfaces and one top surface. Aerodynamic forces are calculated individually with respect to the local airflow at the locations of the two side particles and the top particle. The fourth particle is added to obtain a three dimensional body with rotational inertia. The attachment of the tether that connects kite and drone coincides with the top surface particle. The steering behavior of the kite is modeled by changing the local angle of attacks of the side surfaces differentially proportional to the steering input [11]. This results in a differential change of the aerodynamic forces acting on the side particles which induces a yaw moment that results in a turn rate. The steering behavior model is a great simplification compared to reality, but sufficient for the purpose in this paper. For a more realistic high fidelity model please refer to [12]. The coupled system of differential equations that describes the dynamics of the kite is obtained eventually by applying Newton's second law of motion for every particle point mass.

$$\begin{aligned} \left(\dot{\mathbf{p}}_i\right)_W &= \left(\mathbf{v}_{k,i}\right)_W \\ \left(\dot{\mathbf{v}}_{k,i}\right)_W &= \frac{1}{m_i} \cdot \left(\mathbf{F}_{\Sigma,i}\right)_W \end{aligned} \quad (20)$$

where  $i$  denotes the  $i$ th kite particle and the resultant force is denoted by  $(\mathbf{F}_{\Sigma,i})_W$ . The calculation of the specific forces is discussed in detail in [11] and will not be repeated here. The only additional force that appears in the equations of motion in this work is the tether force transmitted through the tether that connects the quadcopter with the kite, as defined in equation 16. Note that this force is set to zero as soon as the kite is detached from the drone.

### C. Tether

The tether between ground station and kite is modeled as a  $n$ -particle system and is adapted from [11]. The individual segments are modeled as spring-damper elements according to equation 16. In contrast to the connection between the drone and the kite the tether between kite and ground station has a variable length. This will be modeled by simultaneously changing the lengths of the segments during the reel-out phase. Analogously to the kite particles for every tether particle Newton's second law will be applied. For particles  $2 - n - 1$  this yields

$$\begin{aligned} (\dot{\mathbf{p}}^{P,i})_W &= (\mathbf{v}_k)_{P,i} W \\ (\dot{\mathbf{v}}_k^{P,i})_W &= \frac{1}{m_{P,i}} ((\mathbf{F}_{P,i,g})_W + (\mathbf{F}_{P,i,a})_W + \\ &\quad (\mathbf{F}_{s,i-1,t})_W + (\mathbf{F}_{s,i+1,t})_W) \end{aligned} \quad (21)$$

$(\mathbf{F}_{P,i,g})_W$  and  $(\mathbf{F}_{P,i,a})_W$  denote the gravitational and the aerodynamic force for particle  $i$ , respectively. A detailed derivation of these forces can again be found in [11].  $(\mathbf{F}_{s,i-1,t})_W$  and  $(\mathbf{F}_{s,i+1,t})_W$  represent the spring-damper forces of the connecting tether segments. For the first particle  $i = 1$  the lower spring-damper force is replaced by the force as experienced by the winch and for the last particle  $i = n$  the upper spring-damper force is replaced by the three spring-damper forces that model the bridle system.

### D. Ground station

In this work only the mechanical part of the ground station, i.e. the winch, is modeled as a simple scalar second order given by

$$\begin{aligned} \dot{\theta}_w &= \omega \\ \dot{\omega}_w &= \frac{1}{J_w} \left( r_w \left\| (\mathbf{F}_{s,1,t})_W \right\|_2 - \nu_w \dot{\theta}_w + M_c \right) \end{aligned} \quad (22)$$

where  $r_w$  is the drum radius,  $\nu_w$  is the friction coefficient,  $\left\| (\mathbf{F}_{s,1,t})_W \right\|_2$  is the absolute tether force of the first tether segment, and  $M_c$  is the pseudo control moment. The overall tether length is given by

$$l_t = r_w \theta_w \quad (23)$$

## E. Shear Wind Model

In order to simulate the launching and landings maneuvers in a realistic wind environment a Dryden turbulence model has been superimposed to a shear wind field model. Both models are implemented according to MIL-F-8785C for category C flight phases, which incorporate takeoff and landing maneuvers of aircraft. Therefore the model seems to be adequate in the analyzed launching and landing context of this work. According to the specification the shear model is given by

$$v_w = W_{20} \frac{\ln\left(\frac{h}{z_0}\right)}{\ln\left(\frac{20}{z_0}\right)}, \quad (24)$$

where  $W_{20}$  is the wind speed at  $6m$ ,  $h$  is the current altitude in feet and  $z_0 = 0.15$  is a parameter chosen according to the specification. If it is assumed that equation (24) reflects the local wind profile accurately it can also be used to estimate the altitude at which a certain wind speed is expected if no other information about the wind profile is available. In this case it is assumed that  $W_{20}$  is measurable.

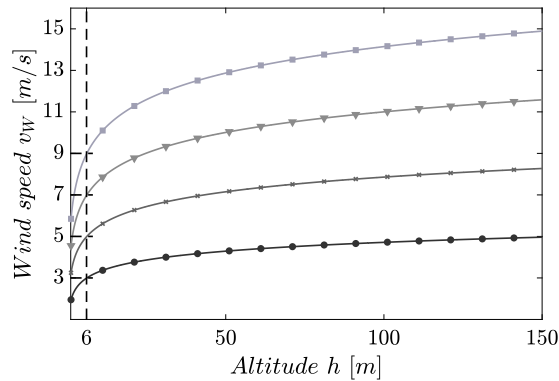


**Fig. 7 Shear wind field according to MIL-F-8785C [13] with  $W_{20} = 3\frac{m}{s}$  (circles),  $W_{20} = 5\frac{m}{s}$  (crosses),  $W_{20} = 7\frac{m}{s}$  (triangles) and  $W_{20} = 9\frac{m}{s}$  (squares). The intersections of the vertical and horizontal dashed lines indicate the reference wind speeds  $W_{20}$  at  $6m$ .**

## IV. Controller Design

### A. Quadcopter Flight Controller

In this section the control strategy will be presented and the control laws will be derived. Overall the launching procedure can be divided into three phases. Note, the drone is assumed to be attached to the kite before take-off. In the first phase the drone lifts off and the kite remains in the initial state until the tether between drone and kite is taut. In the second phase the drone drags the kite along the launching path until the specified operational altitude is reached. At the same time the winch reels out the tether, while the tether length setpoint for the controller is given by the relative distance between the quadcopter and the winch. This ensures that the kite will always keep a minimum distance to the drone to prevent a collision. As soon as the drone reaches the operational altitude the kite will be released and the reeling out speed will be set to zero. The drone will follow the landing path and the kite will reach its parking position according to equation (1). As soon as the drone has landed the launching phase is terminated and the kite goes into power production mode.

The landing maneuver will be carried out inversely. First, the kite will be steered to the parking position. As soon as the kite

reaches the parking position, the kite will be pulled towards the ground station using a force feedback control approach.

For the drone flight control architecture a cascaded structure is chosen. Since highly curved flight paths are not required during the launching and the landing procedure a path following controller that enables the drone to follow straight line segments connected with circular orbits with a defined velocity profile is sufficient. Since the rotational dynamics of the drone are neglected in this work, no inner loop controller is required. However, due to the modularity of the cascade structure an attitude and rate loop can be added effortlessly in the future.

### 1. Path Planner

In this section the launching path will be defined, consisting of straight line segments connected with circle segments to achieve smooth transitions from one line segment to another. The path inclination is chosen such that the kite will be launched below the parking equilibrium elevation angle. The to be expected parking equilibrium angle can be determined based on the results in section II. This will result in a tangential motion towards the parking equilibrium position as soon as the kite is detached from the drone. Since the wind field is not known a priori only bounds on the launching elevation can be given. The general appearance of the reference flight path with a path angle of  $\gamma = 60^\circ$  is depicted in figure 8 where the solid line represents the flight path and the dashed lines complete the circle segments for visualization purpose only. During the first part of the launching phase the drone follows a vertical path before transitioning onto the inclined path segment via two circle segments that start and end tangentially to the adjacent straight line segments. As soon as the drone reaches the release altitude (indicated by the cross) the kite is released and the drone follows another circular orbit and a final straight line descend path segment. To keep the path planning as simple as possible a minimal representation of the reference flight path is developed. More specifically, the path is fully defined by the release altitude  $h_r$ , the path angle of the straight line segment until the release altitude  $\gamma_1$  and the altitude of the initial vertical segment  $h_i$ . The radii  $r_j, j \in \{1, 2, 3\}$  as well as the centers of the circular segments  $(\mathbf{p}_{c,j})_W$  can be calculated based on the following geometric considerations. The first segment is defined by

$$\begin{aligned} r_1 &= h_i \tan\left(\frac{\pi}{4} - \frac{\gamma_1}{2}\right) \\ (\mathbf{p}_{c,1})_W &= \begin{pmatrix} r_1 & 0 & h_i \end{pmatrix}^T \end{aligned} \quad (25)$$

The derivation of  $r_2$  and  $(\mathbf{p}_{c,2})_W$  requires intermediate steps, First, the waypoint between the first and second circle segment is calculated according to

$$(\mathbf{w}_3)_W = (\mathbf{p}_{c,1})_W + \begin{pmatrix} 0 & 0 & r_1 \end{pmatrix}^T \quad (26)$$

The subsequent waypoint can be calculated with

$$(\mathbf{w}_4)_W = (\mathbf{w}_3)_W + \begin{pmatrix} 1 + \cos \gamma_1 \\ 0 \\ \sin \gamma_1 \end{pmatrix}_W \begin{pmatrix} \frac{w_{3,z}}{\tan \gamma_1} - w_{3,x} \end{pmatrix}, \quad (27)$$

where  $w_{3,x}, w_{3,z}$  represent the  $x_W$  and  $y_W$  components of  $(\mathbf{w}_3)_W$ , respectively. Eventually, it follows for the radius and origin of the second orbit:

$$r_2 = \frac{w_{4,x} - w_{3,x}}{\sin \gamma_1} \quad (28)$$

$$(\mathbf{p}_{c,2})_W = (\mathbf{p}_{c,1})_W + \begin{pmatrix} 0 & 0 & r_1 + r_2 \end{pmatrix}_W.$$

where  $w_{4,x}$  is the  $x_W$  component of  $(\mathbf{w}_4)_W$ . The radius and origin of the third orbit can be calculated according to

$$r_3 = \frac{h_r}{\sin \gamma_1} \tan \left( \frac{\pi}{4} - \frac{\gamma_1}{2} \right) \quad (29)$$

$$(\mathbf{p}_{c,3})_W = \begin{pmatrix} r_3 & 0 & \frac{h_r}{\sin \gamma_1} \end{pmatrix}_W^T$$

The remaining waypoints are given by

$$\begin{aligned} (\mathbf{w}_1)_W &= \begin{pmatrix} 0 & 0 & 0 \end{pmatrix}_W \\ (\mathbf{w}_2)_W &= \begin{pmatrix} 0 & 0 & h_i \end{pmatrix}_W \\ (\mathbf{w}_5)_W &= \begin{pmatrix} \frac{h_r}{\tan \gamma_1} & 0 & h_r \end{pmatrix}_W \\ (\mathbf{w}_6)_W &= \begin{pmatrix} 0 & 0 & \frac{h_r}{\sin \gamma_1} \end{pmatrix}_W \end{aligned} \quad (30)$$

Having defined the parameterization of the flight path, the next step will be to determine the path parameters  $h_r$  and  $\gamma_1$  according to the results in section II. First of all, the results displayed in figure 4 suggest that the multicopter assisted launching is only required in low wind conditions on the ground i.e.  $v_w < 8 \frac{m}{s}$ . Since the drone is designed such that it can lift the kite without relying on a minimum wind speed the operational envelope can be enlarged. To frame the control goal a successful drone assisted launch will be defined as such that after the detachment of the kite it has to be able to reach a stable parking equilibrium. This requires that at release altitude the wind speed is higher or equal  $8 \frac{m}{s}$ , which represents a conservative boundary condition indicated by the cross in figure 4 and hence results in a moment equilibrium.

From a methodological point of view, the release altitude can either be determined based on a wind model or on an online estimation of the wind speed at the kite. Note that the wind speed could be estimated based on airdata measurements at the drone. The online estimation of the wind field is not part of this work, hence a model for the wind field is used to predict the release altitude at which  $v_w = 8 \frac{m}{s}$  is to be expected. From figure 7 it can be observed that for low wind speeds e.g.  $W_{20} = 3 \frac{m}{s}$  the required release altitude might become unfeasible. Due to on-board power constraints as given by the design choices presented in section B it is necessary to constrain the maximum release altitude in order not to violate the maximum available flight time given a specific velocity trajectory. In this work the launching phase of the kite is estimated to take at most 180s, which represents a time constraint for the launching phase that can be transformed into a maximum path length requirement. With a launching velocity of 1m/s the maximum launching distance can be calculated to be 180m. Note that this is a conservative bound since it assumes that the drone is

flying with full throttle during the entire launching phase. The constraint for the maximum release altitude is then dependent only on the path angle. As described in the path planning section the path angle is conservatively chosen based on the measured ground wind speed. Assuming ( $\Theta_t = 0$ ) the minimum path angle is approximately  $\gamma_1 = 72^\circ$ , which corresponds to a wind speed of  $v_{w,min} \approx 8 \frac{m}{s}$ . The maximum release altitude is then given by  $h_{r,max} = 180 \sin(\gamma_1) \approx 170m$ .

With the utilized shear wind model as described by equation 24 the minimum reference wind velocity at 6m altitude can be calculated by solving the wind model for  $W_{20}$  with  $v_w = 8m/s$  and  $h_r = 170$ , which yields  $W_{20,min} = 4.76m/s$ . If this is done for different release altitude the results in figure 9 are obtained. Note that the hatched rectangular areas represent unfeasible solutions since they violate the maximum altitude constraint. For the subsequent simulations a theoretical boundary of  $5 \frac{m}{s}$  is chosen since it leads to much lower release altitude of 126m instead of 176m, where it would be required that the drone tracks the velocity command of  $1 \frac{m}{s}$  perfectly, in order not to violate the time constraint of 180s launching time. Note, with the given wind profile this would enlarge the operational launching envelope from 8m/s to 5m/s, conservatively.

For the landing no prescribed landing path is defined. The reason is that only the radial motion of the kite can be controlled actively using the winch. However, from the equilibrium analysis in section II it can be deduced that for  $v_{ro} < 0$  the kite has the tendency to reach an equilibrium elevation angle if the reeling-in speed and the wind speed form a feasible solution. Hence, deviations from this equilibrium due to external disturbances create a motion in  $x_T$  direction. Connecting all the equilibrium points along the wind shear profile from parking altitude to the ground given a certain reeling-in speed, results in a virtual landing flight path that will be followed passively due to the inherent flight physics of the kite. Theoretically, this makes the landing of the kite rather simple if the wind speed is sufficiently high. The landing performance will be assessed in section V in various turbulent wind fields.

## 2. Path-following Controller

The path following problem is subdivided into straight line and circular orbit following, where a logic module switches between the active path segments. The switching is triggered as soon as the drone reaches the current target waypoint. Smooth transitions onto the path are achieved by implementing a virtual target pursuit algorithm. In both cases the current to be followed path segment is defined by the waypoint ahead  $(\mathbf{w}_+)_W$  and the previous waypoint  $(\mathbf{w}_-)_W$ . In case that  $(\mathbf{w}_+)_W$  and  $(\mathbf{w}_-)_W$  are connected with a straight line the path segment vector is given by

$$(\mathbf{s}_*)_W = (\mathbf{w}_+)_W - (\mathbf{w}_-)_W \quad (31)$$

The relative position between the drone and the previous waypoint  $(\mathbf{w}_-)_W$  is given by

$$(\mathbf{p}_{WD})_W = (\mathbf{p}_D)_W - (\mathbf{w}_-)_W \quad (32)$$

In order to calculate the virtual target on the path, the current quadcopter position needs to be projected onto the path. In case a straight line has to be followed, the closest point is simply given by the normal projection, which is given by

$$(\mathbf{p}_{D,\perp})_W = \frac{(\mathbf{p}_{WD})_W^\top \cdot (\mathbf{s}_*)_W}{(\mathbf{s}_*)_W^\top \cdot (\mathbf{s}_*)_W} (\mathbf{s}_*)_W \quad (33)$$

The virtual target that the drone has to follow is then given by

$$(\mathbf{p}_V)_W = (\mathbf{w}^-)_W + \left( \|(\mathbf{p}_{D,\perp})_W\|_2 + \Delta \right) \frac{(\mathbf{s}_*)_W}{\|(\mathbf{s}_*)_W\|}, \quad (34)$$

where  $\Delta$  is a tuning parameter that defines how aggressive the path following controller will guide the drone onto the path. If  $\Delta \rightarrow 0$  the drone will be guided perpendicular onto the path, which results eventually in oscillations around the path due to the inertia of the system. If  $\Delta$  is too large the perpendicular error component will only be reduced slowly. Hence, a trade-off between the two scenarios has to be made.

To determine the position of the virtual target on a circular orbit the following calculations have to be made. First, the current position of the drone will be projected orthogonally into the circle frame:

$$\begin{aligned} (\mathbf{p}_D)_{C,j} &= (\mathbf{p}_D)_W - (\mathbf{p}_{c,j})_W \\ (\mathbf{p}_D)_{C,j}(2) &= 0 \end{aligned} \quad (35)$$

Next, the drone position will be scaled such that it is projected onto the circle. This is simply given by

$$(\mathbf{p}_{D,p})_W = \frac{(\mathbf{p}_D)_{C,j}}{\|(\mathbf{p}_D)_{C,j}\|_2} r_j, \quad (36)$$

which represents the closest point on the circle relative to the current position. In order to obtain the virtual target the projected position has to be rotated by a user specified angle  $\Delta$ . Depending on the objective,  $\Delta$  has to be chosen positive or negative such that the drone follows the orbit in clock- or counter clockwise direction. The virtual target is then given in the wind frame by

$$(\mathbf{p}_V)_W = \begin{pmatrix} \cos \Delta & 0 & \sin \Delta \\ 0 & 1 & 0 \\ -\sin \Delta & 0 & \cos \Delta \end{pmatrix} (\mathbf{p}_{D,p})_W + (\mathbf{p}_{c,j})_W \quad (37)$$

Note that in both cases, straight line and circular orbit following, additional constraint are implemented that ensure that the virtual target is not placed further than the waypoint ahead.

Together with the desired absolute velocity, as defined by the user, and the position of the virtual target the desired bearing vector is given by

$$(\mathbf{v}_c)_D W = v_d \frac{(\mathbf{p}_V)_W - (\mathbf{p}_D)_W}{\|(\mathbf{p}_V)_W - (\mathbf{p}_D)_W\|_2} \quad (38)$$

Based on the desired velocity vector  $(\mathbf{v}_c)_D W$  the required thrust vector that guides the drone onto the path with velocity  $v_d$  can be calculated as follows. The current velocity tracking error and its time derivative are defined as

$$\begin{aligned} (\mathbf{e}_v)_W &= (\mathbf{v}_r)_D W - (\mathbf{v}_k)_D W \\ (\dot{\mathbf{e}}_v)_W &= (\mathbf{a}_r)_D W - (\mathbf{a}_k)_D W \end{aligned} \quad (39)$$

$(\mathbf{a}_k)_D W$  can be substituted by equation (11), where only the known forces will be considered for the derivation of the control law. All the remaining uncertainties are summarized in  $\Delta$  including the induced disturbance by the kite. The resulting path following error dynamics are then given by

$$(\dot{\mathbf{e}}_v)_W = (\mathbf{a}_r)_D W - \frac{1}{m_D} ((\mathbf{F}_{D,g})_W + (\mathbf{F}_{D,p})_W + \Delta). \quad (40)$$

This yields the required thrust vector  $(\mathbf{F}_{D,p})_W$ :

$$(\mathbf{F}_{D,p})_W = m_D ((\mathbf{v}_r)_W - (\mathbf{F}_{D,g})_W), \quad (41)$$

where  $(\mathbf{v}_r)_W$  represents the desired acceleration given by

$$(\mathbf{v}_r)_W = (\mathbf{a}_r)_D W + \mathbf{K}_v (\mathbf{e}_v)_W, \quad (42)$$

with a diagonal positive feedback gain  $\mathbf{K}_v \in \mathbb{R}^{3 \times 3}$  and  $(\mathbf{a}_r)_D W$  the desired acceleration that can be calculated with a first order reference filter i.e.

$$(\mathbf{a}_r)_D W = -\frac{1}{\tau_r} (\mathbf{v}_r)_D W + \frac{1}{\tau_r} (\mathbf{v}_c)_D W, \quad (43)$$

where  $\tau_r$  represents the time constant of the filter, that represent a tuning parameter. The choice of the time constant is usually constraint by the time constants of the inner loop dynamics and the bandwidth of the actuator dynamics. Since both inner loop and actuator dynamics are neglected, no further constraints on  $\tau_r$  need to be imposed.

The pseudo-control law in equation (41) ensures stable error dynamics for bounded disturbances  $\Delta$ , which is trivial to see from equation 44.

$$(\dot{\mathbf{e}}_v)_W + \mathbf{K}_v (\mathbf{e}_v)_W = -\Delta \quad (44)$$

Due to the high forces that the kite can generate it is likely that the drone actuators saturate during the launching and landing

phase. Although actuator dynamics are not implemented in the simulation framework so far, the available thrust is limited based on the drone design decisions in section B. To generate feasible reference trajectories and to prevent integrator windup in case of saturation pseudo-control hedging [14] is implemented.

## B. Kite Attitude Controller

Kite power systems are usually controlled on a sphere, where the radius of the sphere is given by the current distance to the ground station. The course controller tracks a reference course on the moving tangential plane while the winch controller controls the movement in radial direction. During the launching the kite has ideally no tangential movement, which means that the course in the tangential plane is not defined. In fact, the translational movement of the kite is entirely controlled by the winch and the drone. The control objective for the kite controller will be then reduced to the tracking of the tangential plane heading angle  $\Psi_{t,c}$ . Since the kite will be launched in downwind direction it is reasonable to define  $\Psi_{t,c} = 0$ .

Based on experimental data and kinematical relationships a correlation between the steering input and the course rate can be derived [15]. Since the sideslip angle is negligible the heading rate is equal to the course rate, which allows a straightforward adoption of the course rate law to derive the kite attitude controller for the launching and landing phase. From the onboard IMU measurements of the kite it can be assumed that the Euler angles are available as state feedback variables. The tangential plane heading angle that will be tracked during launching and landing can be calculated from the measured Euler angles using the relationship between the different coordinate frames:

$$\mathbf{M}_{TB}(\Psi_t, \Theta_t, \Phi_t) = \mathbf{M}_{TW}(\lambda, \phi) \mathbf{M}_{WO}(\xi) \mathbf{M}_{OB}(\Psi, \Theta, \Phi) \quad (45)$$

In the simulation the orientation of the kite in terms of Euler angles  $\Psi, \Theta$  and  $\Phi$  is given by the relative position of the four particles. An orthonormal basis representing the bodyfixed frame  $B$  is then given by

$$\begin{aligned} (\mathbf{e}_z)_W &= \frac{(\mathbf{p}_0)_W - (\mathbf{p}_1)_W}{\|(\mathbf{p}_0)_W - (\mathbf{p}_1)_W\|} \\ (\mathbf{e}_y)_W &= \frac{(\mathbf{p}_3)_W - (\mathbf{p}_2)_W}{\|(\mathbf{p}_3)_W - (\mathbf{p}_2)_W\|} \\ (\mathbf{e}_x)_W &= (\mathbf{e}_y)_W \times (\mathbf{e}_z)_W \end{aligned} \quad (46)$$

with

$$(\mathbf{p}_0)_W = 0.5 \cdot ((\mathbf{p}_2)_W + (\mathbf{p}_3)_W) \quad (47)$$

The current kite attitude in this work is either given in terms of the Euler angles between the tangential plane frame  $T$  and the body fixed frame  $B$  or as in common aerospace applications as the orientation of the  $B$  frame with respect to the north-east-down frame ( $O$ ). The transformation matrices are given by

$$\mathbf{M}_{BO} = \mathbf{M}_{BW}\mathbf{M}_{WO} = \begin{pmatrix} (\mathbf{e}_x)_W^T \\ (\mathbf{e}_y)_W^T \\ (\mathbf{e}_z)_W^T \end{pmatrix} \begin{pmatrix} \cos \xi & \sin \xi & 0 \\ \sin \xi & -\cos \xi & 0 \\ 0 & 0 & -1 \end{pmatrix}, \quad (48)$$

and

$$\mathbf{M}_{WT} = \begin{pmatrix} -\sin \phi \cos \lambda & -\sin \lambda & -\cos \phi \cos \lambda \\ -\sin \phi \sin \lambda & \cos \lambda & -\cos \phi \sin \lambda \\ \cos \phi & 0 & -\sin \phi \end{pmatrix} \quad (49)$$

where  $\xi$  is the wind direction relative to the north direction. For convenience  $\xi$  will be set to zero in the simulation environment (downwind = north).  $\mathbf{M}_{BT}$  has the same structure as  $\mathbf{M}_{BO}$ , which is defined for instance in [16]). Comparing the general structure with the right hand side allows to determine the the attitude of the kite with respect to the tangential frame as follows:

$$\begin{aligned} \Phi_t &= \arctan2(\mathbf{M}_{BT}(2,3), \mathbf{M}_{BT}(3,3)) \\ \Theta_t &= \arcsin(-\mathbf{M}_{BT}(1,3)) \\ \Psi_t &= \arctan2(\mathbf{M}_{BT}(1,2), \mathbf{M}_{BT}(1,1)) \end{aligned} \quad (50)$$

where  $\mathbf{M}_{BT}(i,j)$  denotes the component of  $\mathbf{M}_{BT}$  in the  $i$ -th row and  $j$ -th column in

The model for the controller synthesis can be derived based on kinematic considerations and the steering to yaw rate correlation presented in [15]. The rotational velocity of the kite frame and the NED frame as measured by the IMU can be expressed as

$$\left(\boldsymbol{\omega}^{\text{TB}}\right)_B = \left(\boldsymbol{\omega}^{\text{TW}}\right)_B + \left(\boldsymbol{\omega}^{\text{WO}}\right)_B + \left(\boldsymbol{\omega}^{\text{OB}}\right)_B \quad (51)$$

The transport rate  $\left(\boldsymbol{\omega}^{\text{OW}}\right)_B$  can be neglected in this application, hence the remaining rates can be written as

$$\begin{pmatrix} p \\ q \\ r \end{pmatrix}_B = \mathbf{M}_{BW} \begin{pmatrix} \dot{\lambda} \sin \phi \\ -\dot{\phi} \cos \lambda \\ \dot{\phi} \end{pmatrix}_W + \begin{pmatrix} \dot{\Phi}_t - \dot{\Psi}_t \sin \Theta_t \\ \dot{\Theta}_t \cos \Phi_t + \dot{\Psi}_t \sin \Phi_t \cos \Theta_t \\ -\dot{\Theta}_t \sin \Phi_t + \dot{\Psi}_t \cos \Phi_t \cos \Theta_t \end{pmatrix}_B \quad (52)$$

In [15] it has been shown that a steering input mainly influences the yaw rate of the kite. Furthermore, note that

$$\begin{aligned} \dot{\lambda} &= \frac{v_k}{\|(\mathbf{p}_K)_W\|_2 \cos \phi} \\ \dot{\phi} &= \frac{u_k}{\|(\mathbf{p}_K)_W\|_2} \end{aligned} \quad (53)$$

where  $u_k$  and  $v_k$  are the x and y component of the kinematic velocity vector of the kite in the tangential plane frame. Since during the launching and the landing phase the movement of the kite in the tangential plane is negligible, it can be assumed that  $\dot{\lambda} \approx \dot{\phi} \approx 0$ . The third row of equation (52) can then be simplified to

$$r = -\dot{\Theta}_t \sin \Phi_t + \dot{\Psi}_t \cos \Phi_t \cos \Theta_t \quad (54)$$

The angle  $\Phi_t$  is usually negligibly small, hence

$$r = \dot{\Psi}_t \cos \Theta_t \quad (55)$$

Using the steering correlation as presented in [15] the model for the tangential plane heading rate is given by

$$\dot{\Psi}_t = \frac{1}{\cos \Theta_t} \left( c_1 v_a u_s + c_2 \frac{(\mathbf{F}_{K,g})^\top (\mathbf{e}^{y,B})_W}{g} \right) \quad (56)$$

where  $(\mathbf{F}_{K,g})^\top (\mathbf{e}^{y,B})_W$  can be calculated based on the attitude of the kite and is given by

$$(\mathbf{F}_{K,g})^\top (\mathbf{e}^{y,B})_W = \cos \Theta \sin \Phi m_k g, \quad (57)$$

$v_a$  is the magnitude of the apparent wind speed at the kite and  $u_s$  is the steering input. The coefficients  $c_1$  and  $c_2$  are calculated based on a linear regression as described in [15] and are kite specific. During the launching and landing phase the roll angle of the kite is close to zero  $\Phi \approx 0$  which simplifies the steering law model significantly. The control law is then given by

$$u_s = \frac{\cos \Theta_t v_{\Psi_t,K}}{c_1 v_a} \quad (58)$$

with  $v_{\Psi_t,K}$  is the pseudo control input defined by

$$v_{\Psi_t,K} = \dot{\Psi}_{t,r} + k_{p,\Psi_t} e_{\Psi_t} + k_{i,\Psi_t} \int_0^t e_{\Psi_t} d\tau \quad (59)$$

with the tracking error  $e_{\Psi_t} = \Psi_{t,r} - \Psi_t$ , control gains  $k_{p,\Psi_t}, k_{i,\Psi_t} > 0$  The reference heading rate given by a scalar first order reference filter

$$\dot{\Psi}_{t,r} = -\frac{1}{\tau_{\Psi_{t,r}}} \Psi_{t,r} + \frac{1}{\tau_{\Psi_{t,r}}} \Psi_{t,c}. \quad (60)$$

The parameter  $c_1$  has to be determined based on experimental data, hence represents a multiplicative uncertainty that the error controller has to account for.

### C. Winch controller

The winch controller is based on the model defined in equation (22). Within the scope of this paper a simple linear quadratic regulator (*lqr*) with servomechanism is chosen [14]. The linear model for the controller synthesis is defined as

$$\begin{pmatrix} \dot{\theta}_w \\ \dot{\omega}_w \\ e_{\theta_w} \end{pmatrix} = \begin{pmatrix} 0 & 1 & 0 \\ 0 & -v_w/J_w & 0 \\ -1 & 0 & 0 \end{pmatrix} \begin{pmatrix} \theta_w \\ \omega_w \\ \int_0^t e_{\theta_w} d\tau \end{pmatrix} + \begin{pmatrix} 0 \\ 1/J_w \\ 0 \end{pmatrix} M_c \quad (61)$$

with  $e_{\theta_w} = \theta_{w,c} - \theta_w$ . The feedback law is then given by

$$M_c = -\mathbf{K}_{\theta_{w,p}} \begin{pmatrix} \theta_w \\ \omega_w \end{pmatrix} + k_{\theta_{w,i}} \int_0^t e_{\theta_w} d\tau \quad (62)$$

with  $\mathbf{K}_{\theta_{w,p}} \in \mathbb{R}^{1 \times 2}$  and  $k_{\theta_{w,i}} \in \mathbb{R}$  are the *lqr* gains. The feedback law allows to control the tether length according to equation (23). The setpoint  $\theta_{w,c}$  is given by the current drone position and the dimensions of the kite and tether connection according to

$$\theta_{w,c} = \frac{1}{r_w} \left( \|(\mathbf{p}_D)_w\|_2 - l_{KD} - h_K - h_B + \Delta_s \right) \quad (63)$$

where  $l_{KD}$  is the constant length of the tether between drone and kite,  $h_K$ , is the height of the kite,  $h_B$  is the length of the bridle system and  $\Delta_s$  is an additional parameter that ensures that the tether is slightly slack during the launching and landing phase. As a safety measure the reeling-out speed will be additionally constrained by the launching velocity.

For the non-assisted launching and landing the tether force is controlled. The setpoint calculation for the reeling out speed is based on a simple state-machine with states  $s = \{s_0, s_1, s_2\}$ . If the measured tether force on the ground exceeds a threshold  $T_{\max,u}$  the state transition  $s_0 \rightarrow s_1$  will be triggered and the current reeling out speed setpoint will be increased until the tether force drops below  $T_{\max,l}$  ( $s_1 \rightarrow s_0$ ), where  $T_{\max,l} < T_{\max,u}$  to avoid chattering. Similarly, if the tether force drops below a specified threshold  $T_{\min,l}$  the transition  $s_0 \rightarrow s_2$  will be triggered and a higher reeling-in speed will be issued until the tether force exceeds  $T_{\min,u}$  ( $s_2 \rightarrow s_0$ ), where  $T_{\min,u} > T_{\min,l}$ . The setpoints for  $v_{ro}$  in each state are calculated according to

$$v_{ro} = \begin{cases} -K_p (|T - T_{\max,l}|) & \text{if } T > T_{\max,l} \wedge s = s_1 \\ K_p (|T - T_{\min,u}|) & \text{if } T < T_{\min,u} \wedge s = s_2, \\ \bar{v}_{ro} & \text{if } T_{\min,l} < T < T_{\max,u} \wedge s = s_0 \end{cases} \quad (64)$$

As long as the tether force is between the maximum and minimal tether force threshold ( $s = s_0$ ) the winch will reel-in or reel-out with the nominal reeling out speed  $\bar{v}_{ro}$  set by the operator, where  $\bar{v}_{ro}$  is either negative or positive during landing and launching, respectively. The speed controller is implemented analogously to the tether length controller. In this case however only the angular velocity commands from the state machine will be tracked.

## V. Results

In this section simulation results will be presented that are used to verify the feasibility of the proposed concept. Furthermore the conservative bounds derived in section II will be verified and their conservatism will be demonstrated, to motivate future research activities. The section is subdivided into two parts. In the first part launching simulations will be discussed and the possible benefits of a drone assisted launching will be analyzed. In the second part results of landing simulations will be presented. The goal of both parts is to detect boundary conditions for vertical takeoff and landing maneuvers for flexible wing kite power systems and to develop a methodology that can be used as a basis for future investigations with refined models and ultimately assessed in real flight tests.

### A. Drone-assisted launching

According to the measured wind speed at the reference altitude  $h_r = 6m$  the launching path angle and the release altitude will be determined based on the results in section 1. The feasibility of the drone assisted launching will be verified at the boundaries using the following numerical simulations.

Setting  $W_{20} = 5 \frac{m}{s}$  and selecting  $h_r = 130$  the results depicted in figure 10 are obtained. Note, that besides the minimum release altitude of  $130m$  also a more conservative release altitude of  $150m$  has been selected and simulated.

The performance of the proposed control strategy is discussed in the following in more detail.

The path following controller is able to track the reference velocity despite the unknown induced disturbance of the kite accurately and hence guides the drone along the predefined flight path robustly in the turbulent wind environment. After the kite is released at  $t = 142s$  the drone accelerates in  $z$  and  $x$  direction slightly, but recovers the tracking performance rapidly. Due to the lack of an aerodynamic model for the drone the only disturbance the controller has to account for is represented by the kite. In the simulation this lead only in the initial lift-off phase to deviations from the reference flight path. After the drone starts following the inclined flight path segment defined by waypoint 4 and 5 the deviations from the flight path are negligible. The initial drone flight path is depicted in figure 12.

It can be observed that as the wind speed increases with higher altitudes the induced disturbance of the kite acting on the drone raises which has to be compensated with more thrust. Eventually this leads to a saturation of the total thrust. Saturation of the control input can usually cause windup issues, which is prevented in this work using pseudo-control hedging that essentially slows down the drone by adapting the generated reference velocity. Note that in the future the flight path could be further optimized such that the aerodynamic force of the kite would be exploited more beneficially to decrease the required thrust of the quadcopter.

Note, the flight path can also be chosen such that the kite will be guided along the equilibrium points given by the wind speed and the launching velocity profile. In this case the tendency of the kite to leave the imposed launching path by the drone can be reduced. However, as has been discussed in section II, higher radial velocities result in higher elevation angles. Hence, after the detachment of the kite a tangential motion towards lower elevation angles will result. This can lead to high angles of attack that are not yet predictable by the model implemented in this work. Therefore this approach has not been further investigated.

As can be observed in figure 14, the heading controller is able to keep the kite pointing towards the zenith position, which is defined by  $\Psi_{t,k} = 0$ .

To sum it up, the simulation results demonstrate that it is feasible to extend the launching envelop from  $v_{w,r,\min} = 8m/s$  to  $v_{w,r,\min} \approx 5m/s$  using the drone assisted launching concept.

### B. Comparison of Assisted vs. Non-assisted Launching with $W_{20} = 8 m/s$ and $h_r = 100 m$ .

In this section the simple mast based, passive, launching concept will be compared with the drone based concept. The mast based concept relies simply on the lifting force of the kite that triggers the launching phase as soon as the lift force exceeds the weight of the kite. This approach obviously relies on sufficiently high wind speeds in ground proximity. As can be observed in figure 5 the wind velocity for a steady-state launching maneuvers has to be higher than  $\approx 8 \frac{m}{s}$ . The corresponding elevation angle and reeling out speed are depicted in figure 5. For the subsequent simulations a reference reeling out speed of  $1 \frac{m}{s}$  is chosen, which requires a mast inclination angle of  $\approx 62^\circ$ , according to 4. The reeling out of the tether is controlled using the force feedback winch controller that will increase or decrease the reeling-out speed such that the tether is always taut, while simultaneously ensuring that the tension does not exceed a defined limit. Besides the turbulence contribution the kite is launched in perfect downwind direction. The results of the numerical simulation are shown in figure 15.

It can be observed that apart from initial oscillations in tangential direction a launching performance similar to the drone assisted case can be achieved. Small changes in the wind speed due to the turbulence lead to motions perpendicular to the virtual launching path. This is due to the fact that the kite is not forced to follow a path, but instead tries to find a new equilibrium elevation angle depending on the current experienced apparent wind speed. Based on these observations, controlling the radial motion of the non-assisted kite during launching represents a feasible alternative to the drone assisted launch in case  $W_{20} >= 8 \frac{m}{s}$ .

Additionally, the conservatism of the minimum wind speed requirement for a non-assisted launch has been assessed by means of simulations with  $W_{20} < 8m/s$  and different nominal reeling-out speeds  $\bar{v}_{ro}$ . Figure 16 shows the results of a non-assisted launching maneuver with  $W_{20} = 7 \frac{m}{s}$ . As expected, high nominal reeling out speeds deteriorate the launching performance due to the decreasing apparent wind speed in a downwind launching approach. Naturally, this effects becomes less significant as the wind speeds increases. This as can be observed in figure 17, which is due to the fact that the decrease of the apparent wind speed with rising reeling-out speeds becomes less significant. In general, the non-assisted kite launch should be carried out with small reeling out speeds, which is essentially only limited by the accuracy of the winch speed controller, as discussed in section II. Speaking differently, from a flight dynamical point of view a lower nominal reeling out speed leads to less oscillatory motions around the radial launching direction compared to a higher reeling out speed in the same wind field.

### C. Landing

In this section the controller performances during the landing will be analyzed. Assisting the landing of the kite with the drone is difficult to achieve, since it requires the drone to re-attach to the kite in the air. Therefore, the automatic landing performance without assistance is analyzed in different wind conditions and with different nominal reeling-out speeds  $\bar{v}_{ro}$ .

Note, that during the time this research was conducted no further design decisions regarding the mast or the reattachment process were available. Therefore the landing phase will be terminated as soon as a defined minimal tether length is achieved.

In the first landing simulation study three different wind fields have been simulated with a nominal reeling in speed of  $\bar{v}_{ro} = -1$ .

In the case of  $W_{20} = 7 \frac{m}{s}$  and  $W_{20} = 10 \frac{m}{s}$  the kite is pulled towards the ground with a constant speed after a short transition phase where the winch accelerates from  $v_{ro} = 0$  to  $v_{ro} = -1 m/s$ , as can be seen in figure 19. The pitch angle in both cases oscillates slightly around  $\approx -5^\circ$  and  $\approx -3^\circ$ , as can be observed in figure 20. The oscillations can be attributed to the turbulence. Both results indicate a quasi-steady motion of the kite. In the low wind speed case i.e.  $W_{20} = 4 \frac{m}{s}$  the winch controller is actively adjusting the reeling speed. The continuous change in apparent wind speed leads eventually to a strong down and up pitching motion, which accelerates the kite forward and backwards resulting in a difficult to predict landing behavior. This results clearly favors a steady landing with constant reeling-in velocity.

As has been discussed in the previous paragraph, in low wind conditions i.e.  $v_w < 8 m/s$  the winch has to actively adapt the reeling-in speed to keep the tether taut. However, this can lead to overshoots with respect to the ground station that result in non-stationary landing motions. This behavior has been predicted theoretically in section II, but can also be observed in the simulation results in figure 19 and 21. Note that despite the associated conservatism of the results depicted in figure 5 with  $\Theta_t = 0$  the minimum wind speed that would lead to a reliable landing is the same as the minimum wind speed required for the non-assisted launching, which is  $v_w = 8 \frac{m}{s}$ . Theoretically this would allow the kite to hover at constant tether length at every altitude during the landing procedure. Reeling in the tether increases the apparent wind speed and hence would only lead to higher tension and eventually to a higher elevation angle. Besides the maximum tension that can be supported by the tether, also the maximum elevation angle  $\beta_{max}$  has to be considered, which can be exceeded if the reeling-in speed is too high. Numerical simulations with  $v_w = 8 \frac{m}{s}$  and different nominal reeling in velocities in combination with the force feedback controller have been conducted to qualitatively demonstrate the upper boundaries for the reeling-in speed. The results are depicted in figure 21. Conservatively speaking, for a wind speed of  $8 \frac{m}{s}$  a reeling-in speed until  $\approx -1.6 \frac{m}{s}$  allows a steady descend of the kite as can be deduced from figure 5. Using the less conservative results from figure 6 a reeling in speed until  $-2 \frac{m}{s}$  can be expected to lead to a steady landing behavior. In this case the equilibrium elevation angle would be  $\beta \approx 90^\circ$ . These theoretical results match very well with the simulation results depicted in figure 21, where the almost vertical (i.e.  $\beta \approx 90^\circ$ ) trajectory indicated by the triangular markers is obtained with a reeling in speed of  $\bar{v}_{ro} = -2 \frac{m}{s}$ . Higher reeling in speeds e.g.  $\bar{v}_{ro} = -3 \frac{m}{s}$  lead to trajectories with  $\beta > 90^\circ$ , as indicated by the diamond shaped markers in figure 21.

From a methodological point of view the nominal reeling-in speed  $\bar{v}_{ro}$  should be based on the measured reference wind speed  $W_{20}$ . Although at the kite higher wind speeds are to be expected this will not violate the equilibrium conditions, as can be observed from figure 5.

In a nutshell, the boundaries for the wind speed  $W_{20}$  and  $\bar{v}_{ro}$  should be determined based on figure 5. However, it has been demonstrated that lower boundaries are possible. In both the launching and the landing case the pitch angle  $\Theta_t$  plays a decisive role in the determination of the equilibrium point and moves the minimum wind speeds to lower values with decreasing negative pitch angles. In the future the pitch angle will be expressed in terms of apparent wind speed, which will allow to calculate less conservative bounds.

## VI. Conclusion

To conclude the paper a short summary of the proposed VTOL methodology for flexible wing kite power systems will be presented. The key assumptions are repeated for convenience: 1) Knowledge of  $C_L(\alpha)$  and  $C_D(\alpha)$  curves of the kite as well as the geometric properties of the kite such as wing area, bridle length and weight, 2) Available wind speed measurement on the ground at 6 m, 3) Availability of a shear wind model that maps altitude to wind speed. 4) Knowledge of the downwind direction.

The launching methodology can be summarized as follows: First, check if for the measured reference velocity  $W_{20}$  a parking equilibrium exists using e.g. figure 4. Since  $\Theta_t$  is not precisely known only a rough estimate of  $\beta^*$  can be made. A more accurate estimation of  $\Theta_t$  is part of the current research. For the following it will be assumed that such an equilibrium exists, otherwise the kite cannot be launched using the presented methodology. Second, check if  $W_{20} > W_{20,min} = 8m/s$ . If this condition is satisfied the kite can be launched using the force based winch controller without drone assistance. As soon as the kite reaches the operational altitude the winch stops reeling out the tether and the kite will be steered into the parking position, which terminates the launching phase. If  $W_{20,min} < 8m/s$ , the drone can be used to drag the kite to the operational altitude  $h_r$ . The operational altitude can be predicted using a shear wind field model as well as the minimum wind speed  $v_W(h_r)$  that fulfills the parking equilibrium condition. Note that usually release altitudes higher than 100m are required from a operational point of view, which means that  $h_{r,min} = 100m$ . At the operational altitude the kite will be released and the reeling out of the tether will be stopped. The drone will continue following the landing path, while the kite stays in the parking position until the drone is landed. After the drone landed the power production cycle is triggered.

The landing methodology is summarized in the following. The landing will be conducted without the drone and it is assumed that the kite is already in the parking position. First, the wind measurement on the ground will be used to check if  $W_{20} > W_{20,min} = 8m/s$ . If this condition is not satisfied a controlled reeling in of the kite towards the mast might be still possible, as has been demonstrated qualitatively by means of simulations. However for wind speeds lower than  $8m/s$  the kite motion is so far not predictable well enough, which creates room for further research. If the condition is satisfied the kite can be reeled in using the tether force feedback controller as demonstrated in the previous section.

Overall the contribution of this paper can be summarized as follows. The presented work is a first step towards a reliable vertical launching and landing methodology for flexible wing kite power systems. The authors propose a hybrid launching concept based on a mast-based launching system in combination with an external multicoper system. The boundary conditions have been derived based on an equilibrium analysis. Moreover, a simulation framework has been developed consisting of mathematical models for winch, tether, kite and drone. Flight controllers for kite and drone as well as two different winch controllers have been presented. A first feasibility check of the proposed methodology has been carried out by means of numerical simulations in different turbulent wind fields. The results of these simulations comply with the equilibrium analysis and demonstrate the general feasibility of the proposed concept. In the future the mathematical models both for the simulation as well as the equilibrium analysis will be refined and ultimately flight tests will be used to verify the methodology.

## Acknowledgments

This research has been supported financially by the project AWESCO (H2020-ITN-642682), funded by the European Union's Horizon 2020 research and innovation program under the Marie Skłodowska-Curie grant agreement No. 642682.

## References

- [1] Ahrens, U., Diehl, M., and Schmehl, R. (eds.), *Airborne Wind Energy*, Green Energy and Technology, Springer, Berlin Heidelberg, 2013. doi:10.1007/978-3-642-39965-7.
- [2] <http://www.kitemill.no>, accessed November 21, 2017.
- [3] <https://x.company/makani/>, accessed November 21, 2017.
- [4] <http://twingtec.ch/>, accessed November 21, 2017.
- [5] <http://www.e-kite.com/>, accessed November 21, 2017.
- [6] Fagiano, L., and Schnez, S., “On the Take-off of Airborne Wind Energy Systems Based on Rigid Wings,” *Renewable Energy*, Vol. 107, 2017, pp. 473–488. doi:10.1016/j.renene.2017.02.023.
- [7] <http://www.skysails.info/>, accessed November 29, 2017.
- [8] Haug, S., “Design of a Kite Launch and Retrieval System For a Pumping High Altitude Wind Power Generator,” Master’s thesis, University of Stuttgart, 2012. doi:10.18419/opus-3936.
- [9] <http://www.kitegen.com/en/>, accessed November 29, 2017.
- [10] Bauer, F., Hackl, C. M., Smedley, K., and Kennel, R., “On Multicopter-Based Launch and Retrieval Concepts for Lift Mode Operated Power Generating Kites,” *Book of Abstracts of the International Airborne Wind Energy Conference 2015*, edited by R. Schmehl, Delft University of Technology, Delft, The Netherlands, 2015, pp. 92–93. doi:10.4233/uuid:7df59b79-2c6b-4e30-bd58-8454f493bb09.
- [11] Fechner, U., van der Vlugt, R., Schreuder, E., and Schmehl, R., “Dynamic Model of a Pumping Kite Power System,” *Renewable Energy*, Vol. 83, 2015, pp. 705–716. doi:10.1016/j.renene.2015.04.028.
- [12] Bosch, A., Schmehl, R., Tiso, P., and Rixen, D., “Dynamic nonlinear aeroelastic model of a kite for power generation,” *AIAA Journal of Guidance, Control and Dynamics*, Vol. 37, No. 5, 2014, pp. 1426–1436. doi:10.2514/1.G000545.
- [13] “Flying Qualities of Piloted Airplanes,” U.S. Military Specification MIL-F-8785C, November 5, 1980.
- [14] Lavretsky, E., and Wise, K. A., *Robust and adaptive control*, Springer-Verlag London, 2013. doi:10.1007/978-1-4471-4396-3.
- [15] Jehle, C., and Schmehl, R., “Applied Tracking Control for Kite Power Systems,” *AIAA Journal of Guidance, Control, and Dynamics*, Vol. 37, No. 4, 2014, pp. 1211–1222. doi:10.2514/1.62380.
- [16] Stevens, B. L., Lewis, F. L., and Johnson, E. N., *Aircraft control and simulation*, Wiley, Hoboken, New Jersey, 2016. doi:10.1002/9781119174882.

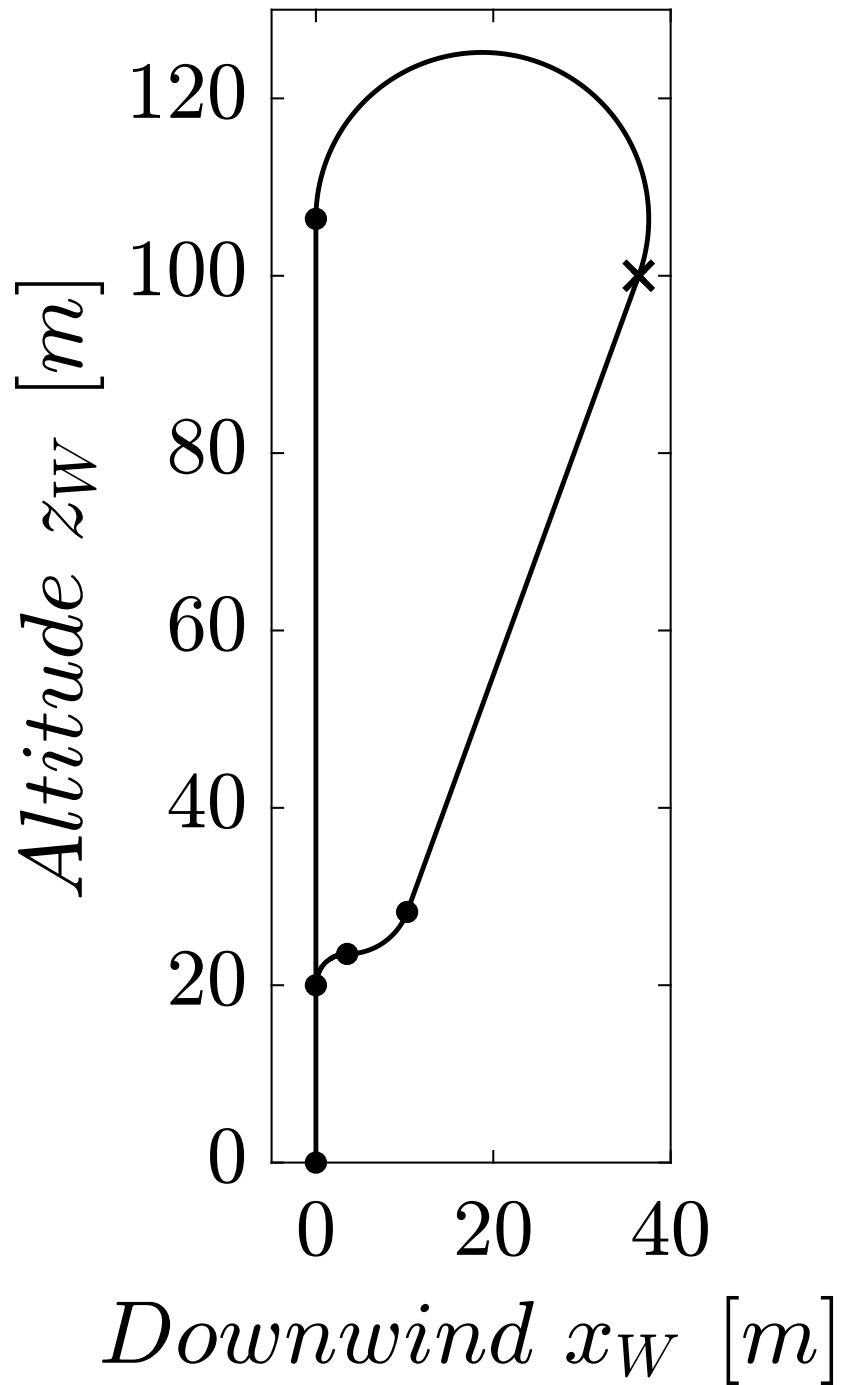


**Fig. 8** The reference launching path consists of straight line and circle segments and is displayed in this figure in the  $x_W z_W$ -plane. The waypoints are indicated by the circular markers. The waypoint indicated by the cross represents the waypoint at which the kite will be detached from the drone. In the displayed case a release altitude of  $h_r = 100m$  is chosen

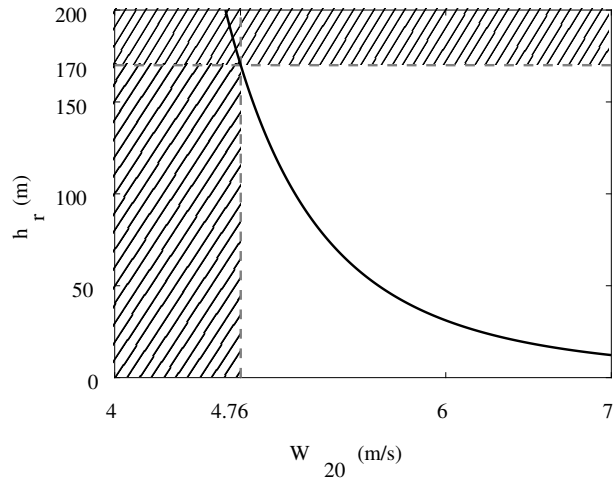


**Fig. 9** Required launching altitude  $h_r$  that would lead to  $v_w = 8 \frac{m}{s}$  and corresponding reference wind speed  $W_{20}$ . The hatched rectangular areas indicate unfeasible combinations of  $W_{20}$  and  $h_r$  that would not enable a kite launching using the proposed concept. For the designed quadcopter the maximum release altitude is  $170m$  which limits the minimum  $W_{20}$  to  $4.76 \frac{m}{s}$ . The curve indicated by the solid line is obtained by solving equation (24) for  $h_r$ , setting  $v_w = 8 \frac{m}{s}$  and evaluating the resulting equation for different  $W_{20}$ .

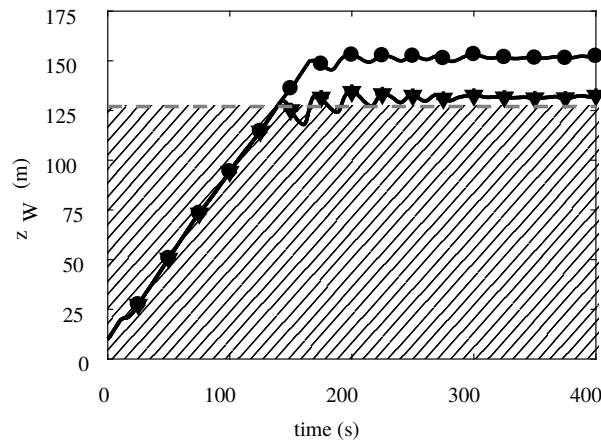


**Fig. 10** Kite altitude trajectory in turbulent wind field with  $W_{20} = 5 \frac{m}{s}$  with release altitude  $h_r = 130m$  (triangles) and release altitude  $h_r = 150m$  (circles).

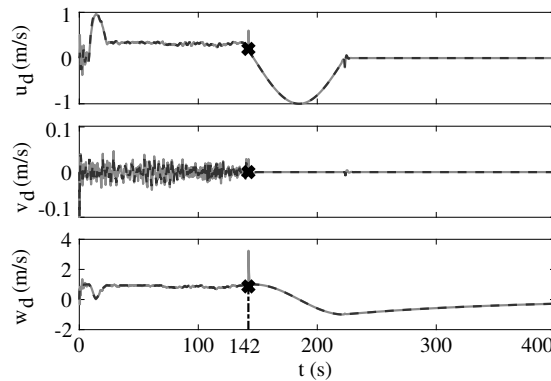


**Fig. 11** Reference velocity tracking performance of the quadcopter path following controller with  $W_{20} = 5 \frac{m}{s}$  and  $h_r = 130m$ . The reference velocity components are indicated by the dashed lines, the real velocity components of the quadcopter are indicated by the solid lines. The cross at  $t = 142s$  indicates the release moment of the kite. All velocity components are given in the wind frame

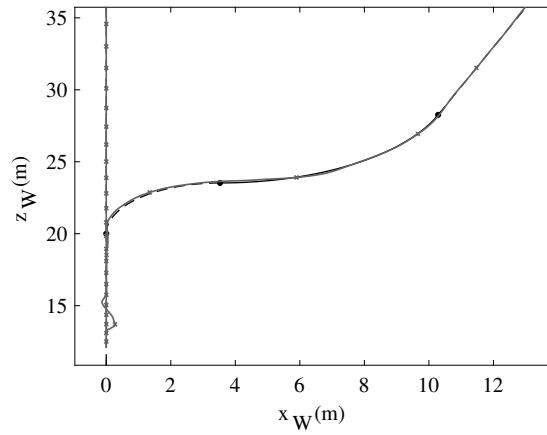


**Fig. 12** Path following performance during the initial and final approach phase of the drone based launching in the  $x_W z_W$ -plane. The reference flight path is given by the dashed line. The actual drone flight path is indicated by the solid line with cross markers.

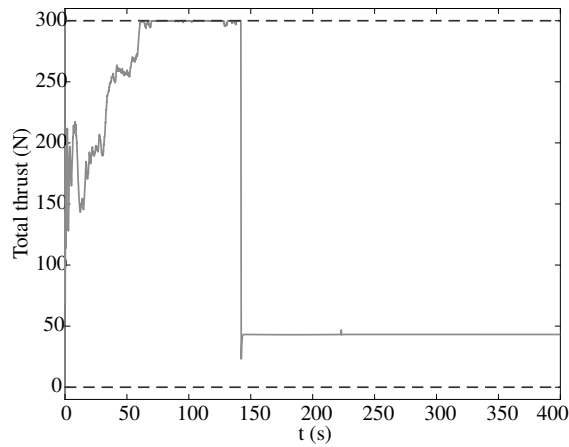


**Fig. 13** Control effort in terms of the total thrust with  $W_{20} = 5 \frac{m}{s}$  and  $h_r = 130m$ . The dashed lines indicate the upper and lower thrust limit.

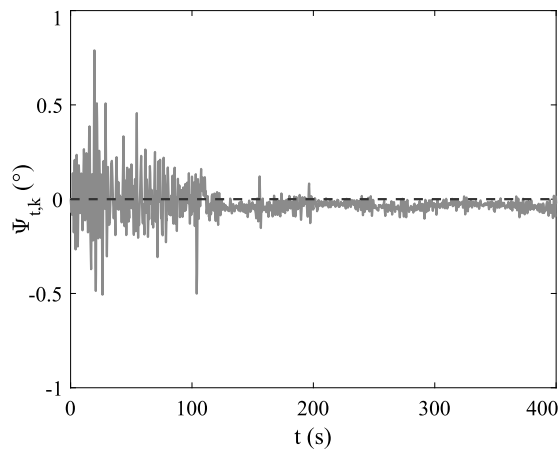


**Fig. 14** Performance of the kite tangential heading controller with  $W_{20} = 5 \frac{m}{s}$  and  $h_r = 130m$ . The current heading in the tangential plane  $\Psi_{t,k}$  is indicated by the solid line, the reference heading is indicated by the dashed line.

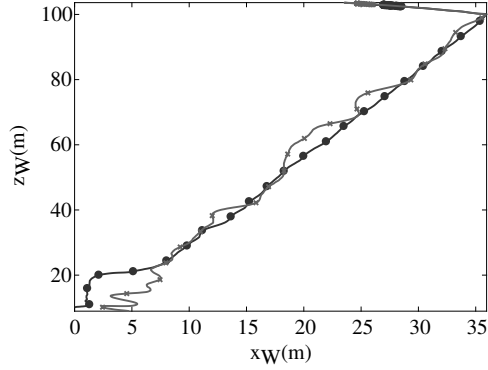


**Fig. 15** Comparison of assisted launching (circles) and non-assisted (crosses) launching maneuver with force control. The wind field parameter  $W_{20}$  and release altitude  $h_r$  are chosen to be  $8 \frac{m}{s}$  and  $100m$ , respectively. To comply with the equilibrium condition the non-assisted kite is launched with an initial inclination of  $62^\circ$

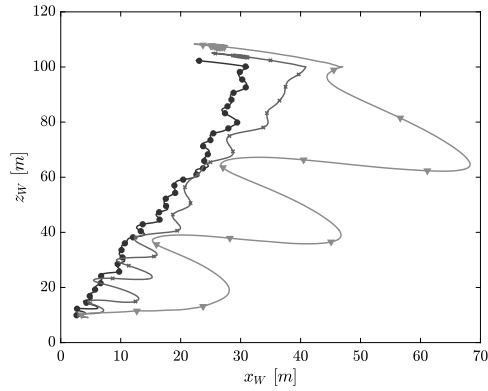


**Fig. 16** Non-assisted launching maneuver with reference wind speeds  $W_{20} = 7 \frac{m}{s}$  and  $h_r = 100m$ . Depicted are trajectories with different nominal reeling out speeds:  $\bar{v}_{ro} = 0.5 \frac{m}{s}$  (circles),  $\bar{v}_{ro} = 1 \frac{m}{s}$  (crosses) and  $\bar{v}_{ro} = 2 \frac{m}{s}$  (triangles).

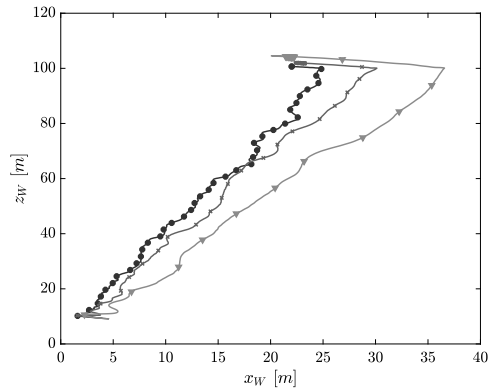


**Fig. 17** Non-assisted launching maneuver with reference wind speeds  $W_{20} = 10 \frac{m}{s}$  and  $h_r = 100m$ . Depicted are trajectories with different nominal reeling out speeds:  $\bar{v}_{ro} = 0.5 \frac{m}{s}$  (circles),  $\bar{v}_{ro} = 1 \frac{m}{s}$  (crosses) and  $\bar{v}_{ro} = 2 \frac{m}{s}$  (triangles).

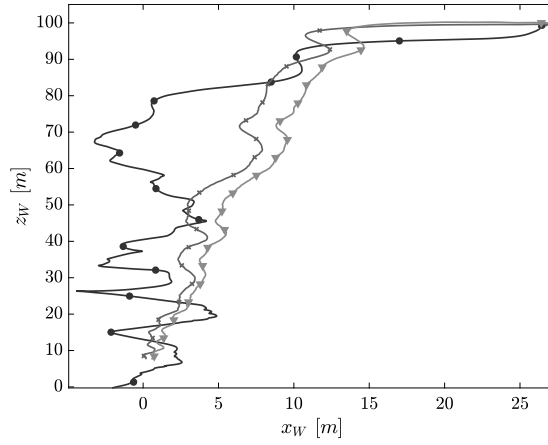


**Fig. 18** Landing of the kite with reference wind speeds, parking altitude  $h_p = 100m$  and tether force feedback controller during reel-in. The path with circular markers represents the landing path of the kite for  $W_{20} = 4 \frac{m}{s}$ , the path indicated by the crosses is obtained for  $W_{20} = 7 \frac{m}{s}$  and the path indicated by the triangles is obtained with  $W_{20} = 10 \frac{m}{s}$

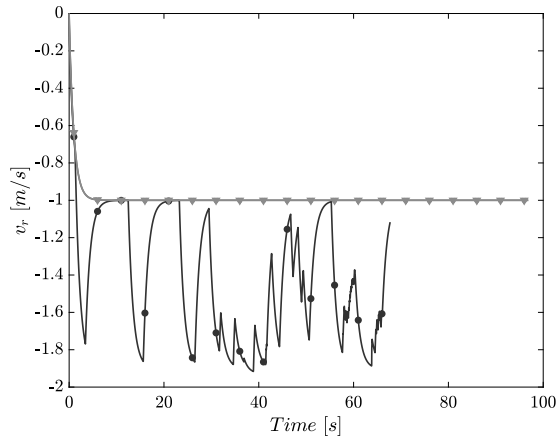


**Fig. 19** Landing of the kite with reference wind speeds, parking altitude  $h_p = 100m$  and tether force feedback controller during reel-in. The circular marker indicates  $W_{20} = 4 \frac{m}{s}$ , the crosses indicate  $W_{20} = 7 \frac{m}{s}$  and the triangles indicate  $W_{20} = 10 \frac{m}{s}$

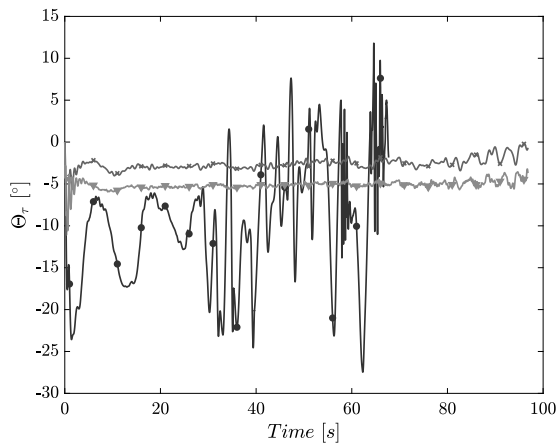


**Fig. 20** Landing of the kite with reference wind speeds, parking altitude  $h_p = 100m$  and tether force feedback controller during reel-in. The circular marker indicates  $W_{20} = 4 \frac{m}{s}$ , the crosses indicate  $W_{20} = 7 \frac{m}{s}$  and the triangles indicate  $W_{20} = 10 \frac{m}{s}$

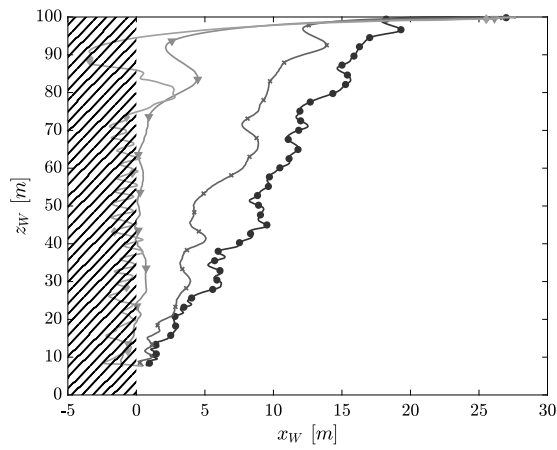


**Fig. 21** Landing of the kite with  $W_{20} = 8 \frac{m}{s}$  for different nominal reeling in speeds:  $\bar{v}_{ro} = -0.5 \frac{m}{s}$  (circles),  $\bar{v}_{ro} = -1 \frac{m}{s}$  (crosses),  $\bar{v}_{ro} = -2 \frac{m}{s}$  (triangles) and  $\bar{v}_{ro} = -3 \frac{m}{s}$  (diamonds). The hatched rectangular area indicates undesired elevation angles  $\beta > 90^\circ$ .